


Article

Uptake of Silver by Jarosite and Natrojarosite Family Compounds at 22 °C, 97 °C and 140 °C

Peter F. Cogram ¹, Mark D. Welch ² and Karen A. Hudson-Edwards ^{3,*} ¹ Department of Earth and Planetary Sciences, Birkbeck, University of London, Malet St., London WC1E 7HX, UK² Department of Earth and Planetary Sciences, The Natural History Museum, London SW7 5BD, UK³ Camborne School of Mines, University of Exeter, Penryn TR10 9FE, UK

* Correspondence: k.hudson-edwards@exeter.ac.uk; Tel.: +44-(0)1326-259-489

Abstract: The jarosite family of minerals are part of the alunite supergroup with the general formula $AB_3(TO_4)_2(OH)_6$. Jarosite family minerals are known to incorporate silver (Ag), but the extent to which this occurs, and at what temperature range, is not well constrained. To address this knowledge gap, jarosite compounds with the A site filled with K, Na, Ag and H_3O were synthesised at 22 °C, 97 °C and 140 °C to simulate low-, moderate- and high-temperature environments, respectively. The compounds were characterised by XRD, SEM, chemical analysis and Raman spectroscopy. All of the synthesised compounds took up Ag. In general, higher temperatures of synthesis increased alkali and Ag occupancy of the A site of the products. Silver contents increased with the increasing concentration of Ag in the starting solutions at all temperatures. The order of preference for occupancy of the A site in the synthesised solids is $K > Na > H_3O > Ag$ at all temperatures, which is consistent with the reported order of ΔG_f of -3309 kJ/mol, -3270 kJ/mol, -3247 kJ/mol and -2948 kJ/mol for jarosite, natrojarosite, hydroniumjarosite and argentojarosite, respectively. The results of this study show that Ag can be incorporated in jarosite and natrojarosite at low-to-high temperatures, and therefore, jarosite family minerals can be important stores of Ag in natural and engineered environments.

Keywords: jarosite; natrojarosite; argentojarosite; hydroniumjarosite; silver; synthetic; XRD; Raman; 22 °C; 97 °C; 140 °C



Citation: Cogram, P.F.; Welch, M.D.; Hudson-Edwards, K.A. Uptake of Silver by Jarosite and Natrojarosite Family Compounds at 22 °C, 97 °C and 140 °C. *Metals* **2023**, *13*, 627. <https://doi.org/10.3390/met13030627>

Academic Editor: Andrii Kostyryzhnev

Received: 15 February 2023

Revised: 10 March 2023

Accepted: 14 March 2023

Published: 21 March 2023



Copyright: © 2023 by the authors. Licensee MDPI, Basel, Switzerland. This article is an open access article distributed under the terms and conditions of the Creative Commons Attribution (CC BY) license (<https://creativecommons.org/licenses/by/4.0/>).

1. Introduction

The alunite supergroup consists of more than 40 minerals with the general formula $AB_3(TO_4)_2(OH)_6$, where A represents cations with a coordination number greater than or equal to 9, and B and T represent cation sites with octahedral and tetrahedral coordination, respectively [1,2] (Figure 1). In an ideal jarosite $[KFe_3(SO_4)_2(OH)_6]$, the B site cation is Fe^{3+} , the A site is occupied by K^+ in 12-fold coordination, and the T site is filled with S^{6+} , forming a sulfate anion (SO_4^{2-}) (Figure 1). The A site can also be filled by Na, forming natrojarosite $[NaFe_3(SO_4)_2(OH)_6]$, or by hydronium (H_3O^+), forming end-member $[(H_3O)Fe_3(SO_4)_2(OH)_6]$. In non-stoichiometric jarosites where there are deficiencies in A-site occupancy, studies often assume the site is occupied by hydronium [3], but H_3O^+ is not necessarily present and there may be vacancies in the site [4]. In addition, a vacancy in the B site may be compensated for by the addition of 4 H^+ (protonation) at the B site, so H_3O in the A site is not necessary for charge balance, hence, vacancies in the A site are commonly seen [5]. These considerations have resulted in a modified general chemical formula being proposed for jarosite compounds: $A_{1-x}(H_3O)_xFe_{3-y}[(OH)_{6-3y}(H_2O)_{3y}(SO_4)_2]$ [6].

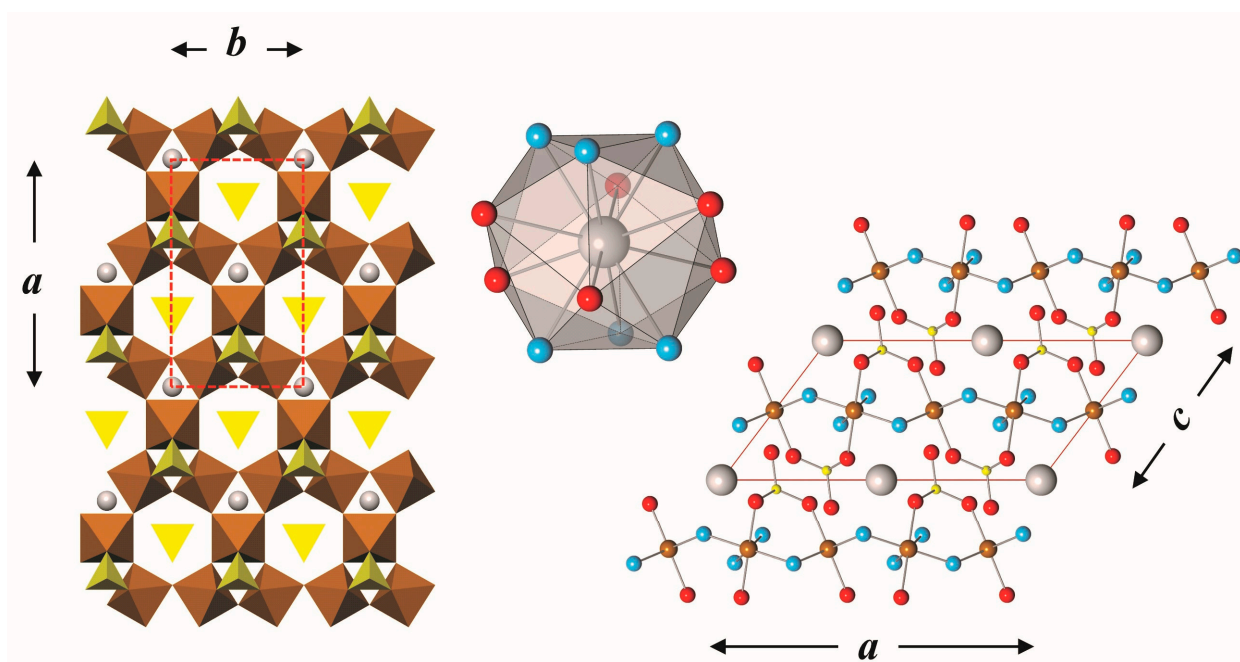


Figure 1. The structure of Na/K/Ag jarosite (monoclinic, space group $C2/m$). Left: A polyhedral representation of the B layer of edge-sharing Fe(OH)₄O₂ octahedra and an overlying SO₄ ... A(Na, K, Ag) layer. Right: Ball-and-spoke diagram showing the alternating layers of Fe(OH)₄O₂ octahedra (Fe brown) and SO₄ tetrahedra (S yellow). Oxygen atoms of hydroxyl groups are shown in pale blue, other oxygen atoms are red. Na/K/Ag atoms are grey. The apical oxygen of the SO₄ tetrahedron (S=O) receives three hydrogen bonds from three hydroxyl groups. The three oxygen O_{donor}(-H) ... O_{acceptor} distances are ~2.75 Å (two) and ~2.95 Å (one). H atoms are omitted for clarity. Centre: A-site atoms (Na/K/Ag) occupy large dodecahedral cavities within the polyhedral framework and are located in the SO₄ layer. (b) The coordination polyhedron of Na/Ag-O₆(OH)₆. Projections of the jarosite unit cell are shown in red.

Solid wastes generated from the processing or natural weathering of sulfide ores can contain precious metals such as silver that escaped extraction or were mobilised in the natural environment. Silver can completely substitute in the A site of the jarosite structure, forming end-member argentojarosite [AgFe₃(SO₄)₂(OH)₆]. Several studies have explored how Ag is incorporated in jarosite and natrojarosite [7–13], and some have shown the existence of a K-Ag-jarosite solid solution series in the presence of hydronium [14]. However, none have explored the possibility of a Na-Ag-(H₃O)-jarosite solid solution series, nor compared the capacity of Ag uptake in natrojarosite and jarosite compounds synthesised at a low temperature (22 °C, ‘room’ temperature and the average surface temperatures in areas where natural jarosites form) with medium (97 °C) or high (140 °C) temperatures typical of hydrothermal systems or metallurgical processes. Such knowledge is important for predicting the ways that Ag can be released from jarosite for the recycling of mine wastes and for predicting the environmental behaviour of Ag-bearing jarosite minerals. To this end, the aims of this study are to determine and compare the capacity of synthetic natrojarosite and jarosite compounds for Ag, the characters of the Ag-bearing jarosite compounds synthesised and the influence of synthesis temperature on these characteristics.

2. Materials and Methods

2.1. Synthesis of Jarosite Compounds

Jarosite group compounds with A sites filled with K, Na, Ag and H₃O were synthesised in 10 series using the volumes, reagents and temperatures listed in Table 1. The initial pH value of each solution was adjusted to 1.5–1.6 by the addition of H₂SO₄ or LiCO₃. The prepared compounds were poured into polypropylene beakers, covered with filter

paper and left for 12–16 months at room temperature (22 °C, to simulate laboratory room temperatures and Earth-surface environments) or poured into Teflon-lined steel vessels and heated to 97 °C or 140 °C in an oven (to simulate hydrothermal and metallurgical environments). During the syntheses at room temperature, the pH of each solution was monitored periodically and adjusted to ensure the value was 1.0–1.6. The precipitate formed was filtered, washed in ultra-pure water (18 MΩ cm^{−1}) and dried at 22 °C (22 °C experiments) and 110 °C (97 °C and 140 °C experiments). These temperatures are typical of those used in other jarosite synthesis studies. The reagents used in the syntheses were AnalaR Normapur or Alfa Aesar grade.

Table 1. Conditions of the synthesis of synthetic jarosite group compounds.

Compound	Solution Volume	Reagents K/Na + Ag	Fe	T of Synthesis (°C)	Temperature of Drying /Annealing	Duration
K-Ag	100 mL	0.11–0 M K ₂ SO ₄ and 0–0.11 M Ag ₂ SO ₄ (5-step series)	0.51 M Fe ₂ (SO ₄) ₃ ·5H ₂ O	22	22 °C	12 months
Na-Ag	100 mL	0.11–0.0275 M Na ₂ SO ₄ and 0–0.0825 M Ag ₂ SO ₄ (3-step series)	0.51 M Fe ₂ (SO ₄) ₃ ·5H ₂ O	22	22 °C	12 months
Ka-Ag	100 mL	0.11–0 M K ₂ SO ₄ and 0–0.11 M Ag ₂ SO ₄ (5-step series)	0.51 M Fe ₂ (SO ₄) ₃ ·5H ₂ O	97	110 °C for 1 h	4 h
Na-Ag	100 mL	0.11–0.0275 M Na ₂ SO ₄ and 0–0.0825 M Ag ₂ SO ₄ (5-step series)	0.51 M Fe ₂ (SO ₄) ₃ ·5H ₂ O	97	110 °C for 1 h	4 h
Ka-Ag	100 mL	0.06–0 M K ₂ SO ₄ and 0–0.06 M Ag ₂ SO ₄ (7-step series)	0.51 M Fe ₂ (SO ₄) ₃ ·5H ₂ O	140	110 °C for 1 h	4 h
Na-Ag	100 mL	0.06–0.01 M Na ₂ SO ₄ and 0–0.05 M Ag ₂ SO ₄ (7-step series)	0.51 M Fe ₂ (SO ₄) ₃ ·5H ₂ O	140	110 °C for 1 h	4 h

2.2. X-ray Diffraction

Powder X-ray diffraction (XRD) analysis of the samples was carried out by collecting patterns in Bragg–Brentano reflection geometry using a Philips PW1876 powder diffractometer (Philips, Amsterdam, the Netherlands) and analysing with PC-APD software (version 1, Philips, Amsterdam, the Netherlands) and X'Menu graphics software (version 1, Malvern Panalytical, Malvern, UK). The anode material used was Cu, which has a Kα₁ wavelength of 1.54056 Å and Kα₂ wavelength of 1.54439 Å, and the α₂/α₁ radiation intensity ratio was 0.5. The generator tension was 40 kV, the current was 30 mA and the instrument was operated at room temperature. The X-ray tube was a long fine-focus type (0.8 mm × 12 mm) and a monochromator was used. Continuous X-ray scans were used, which had a start angle of 10.01° 2θ and an end angle of 69.97° 2θ, a step size of 0.02° 2θ and a time per step of 1.0 s. Before analysis, each sample was ground into a powder using a mortar and pestle.

XRD patterns produced from the samples were compared with reference patterns in the Joint Committee for Powder Diffraction Spectrometry (JCPDS) database. The JCPDS patterns were jarosite 10-0443 and (synthetic) 22-0827; hydroniumjarosite (synthetic) 36-0427; natrojarosite 11-0302, 30-1203 and (synthetic) 36-0425; argentojarosite (synthetic) 25-1327 and 41-1398; and hydroniumjarosite (synthetic) 21-0932 and 31-0650. Cu radiation (Kα₁ λ = 1.54056 Å) was used to produce the profiles from the samples, which all contained Al peaks from the diffractometer's sample holder; these peaks were at ~38.40° 2θ (Kα₁ d-value ~2.34) and ~44.60° 2θ (Kα₁ d-value ~2.03) [15].

A problem that is caused by the use of Cu radiation for the XRD analysis of Fe-bearing minerals such as jarosite is that the X-rays are strongly absorbed, causing a loss of X-ray intensity and high backgrounds as a result of fluorescence. This problem makes the identification and quantification of Fe-rich phases difficult using Cu radiation. For this reason, CoK α ($\lambda = 1.78890$ Å) or FeK α ($\lambda = 1.93604$ Å) X-ray radiation is preferable for Fe-rich phases. Relatively high background intensities were especially noticeable, for example, in the XRD results of JS24, JS26, JS28, JS30, JS49, JS55, JS60, JS72 and JS78. For these samples, additional XRD analysis was carried out using a PANalytical X'Pert Pro diffractometer (Malvern Panalytical, Malvern, UK) with a graphite monochromator. The instrument was fitted with an MPPC generator, PW3376/00 X-ray tube, PW3064 reflection-transmission spinner, PW3050/60 goniometer, X'Celerator detector, X'Pert Data Collector, Data Viewer and Database32, and X'Pert HighScore Plus software version 1. The instrument was operated at room temperature. Co radiation (K α_1 $\lambda = 1.78897$ Å, K α_2 $\lambda = 1.79285$ Å and α_2/α_1 intensity ratio = 0.5) was used for the analyses of the synthesised samples, which were run in reflection mode, and a graphite monochromator I was used. Continuous X-ray scans were used with a start angle of 10.00° 2θ and an end angle of 100.00° 2θ , a step size of 1.00° 2θ and a time per step of 40.0 s, except for the additional scans of two samples using a time per step of 80 s. Before analysis, each sample was ground into a powder using a mortar and pestle.

2.3. Chemical Analysis

For the quantitative total elemental analysis of the Ag-bearing jarosite compounds, approximately 90 mg of each dried synthetic compound was dissolved by adding 3 mL of HF (38 wt. %) plus 1 mL of HNO₃ (67 wt. %) in a Savillex vial with cap and heated at 150°C for 16 h. The resulting solutions were then evaporated at 110°C to incipient dryness. Subsequently, 1 mL of HNO₃ was added to each, and the resulting solutions were evaporated at 110°C to incipient dryness. Following this, 3 mL of HNO₃ and 1 mL of ultra-pure water were added. After digestion, the solutions were made up to 100 mL with ultra-pure water. Following the acid digestion procedure, no visible solid remained. Following this, 10 mL of each solution was put in a 50 mL vial by pipette and 40 mL of ultra-pure water was added. The resulting solutions were analysed for Ag, Na, K, Fe and S by inductively coupled plasma atomic emission spectrometry (ICP-AES) on a Varian 720-ES instrument (Varian, Baden, Switzerland) fitted with both a monochromator and a polychromator.

2.4. Scanning Electron Microscopy

Scanning electron microscopy (SEM) with secondary electron imaging (SEI) was used to determine the crystal morphology of the synthetic jarosite compounds. The SEM analysis was carried out using a Jeol JSM-6480LV Variable Pressure Analytical Scanning Electron Microscope (SEM) (Jel, Tokyo, Japan) with a high resolution of 3.0 nm, equipped with Oxford Link EDS system and electron backscatter diffraction (EBSD) system (Oxford Instruments, Oxford, UK), and using Co K α radiation. The synthetic jarosite compounds were mounted on Leit carbon double-sided adhesive tabs on 5 mm-diameter aluminium stubs and then coated with Au. A cobalt sample was used to calibrate the SEM. Secondary electron imaging of Au-coated samples using 7 kV accelerating voltage, 3.0 μm spot size and a working distance (WD) of 11 mm was used to obtain high-quality images of the synthetic jarosite compounds.

2.5. Raman Spectroscopy

Laser Raman microspectroscopic analyses were carried out using a Renishaw RM1000 Raman spectrometer (Renishaw, Wotton-under-Edge, UK) and other analyses used a Renishaw inVia Raman spectrometer (Renishaw, Wotton-under-Edge, UK), both of which were equipped with a thermoelectrically cooled charge coupled device (CCD) detector and a 514.5 nm Ar ion laser. The instruments were calibrated daily on a silicon standard at

520.5 cm^{-1} . The Renishaw RM1000 system was operated in confocal mode with the laser focused on the sample through the objective lens (magnification 50 \times) of an Olympus petrological microscope, and the Renishaw inVia system used a Leica DM2500 M microscope (Renishaw, Wotton-under-Edge, UK). Under these conditions, the laser beam for analysis was restricted to an area of <2 μm diameter. The initial sample burn at 100% because of the hydrous content of the samples meant that the laser beam power of the Renishaw RM1000 system was reduced from 100% to 25%. The laser power was reduced using neutral density filters and was typically between 1 mW and ~220 μW at the sample surface. The laser beam power of the Renishaw inVia system was reduced to 10% and was 6.76 mW at the sample surface. Following the reduction in beam power, the samples were inspected optically for any laser damage and none was observed.

Spectra were recorded over the frequency range 100 to 4000 cm^{-1} , using integration times of 60 s (except 120 s for one sample). The errors on the spectra were <0.1 cm^{-1} . Peak fitting was performed using Galactic GRAMS/32 software (version 1, Galactic, Bradford, UK) with the Renishaw RM1000 spectrometer (Renishaw, Wotton-under-Edge, UK) and WIRE 3.3 software (version 1, Renishaw, Wotton-under-Edge, UK) with the Renishaw inVia spectrometer (Renishaw, Wotton-under-Edge, UK), both of which use a mixed Gaussian–Lorentzian curve. Depending on the quality of the spectra, between one and four spectra were obtained over the full frequency range. The variation between the different spectra of individual samples was small, and therefore, the samples were assumed to be homogeneous.

3. Results and Discussion

3.1. Morphology of Synthetic Jarosite Compounds

The end members K-H₃O-jarosites, Na-H₃O-jarosites and Ag-H₃O-jarosites synthesised at 22 °C, 97 °C and 140 °C have distinctive morphologies (Figure 2). K-Ag and Na-Ag jarosite solid solutions display transitional forms between the end-member morphologies (images not shown). Crystal sizes increase as the synthesis temperatures increase. K-H₃O jarosite crystals generally comprise rounded hexagonal plates on {0001} [15] and discs, usually intergrown and in compact texture, with grain sizes of 1–20 μm , and as aggregates. The K-H₃O end-member jarosites synthesised at 140 °C have intergrown dipyramidal rhomb morphologies (Figure 2). Na-H₃O jarosite crystals are intergrown with pyramidal {01–12} and {0001} faces and rhombohedral {01–12} faces, in compact texture, with grain sizes of 1–20 μm . Ag-H₃O jarosite crystals comprise intergrown hexagonal plates on {0001} and dipyramidal (octahedral) rhombs with {01–12} and {0001} faces [16], both sometimes rounded, and in compact texture, with grain sizes of 4–25 μm .

3.2. X-ray Diffraction Analysis of Synthetic Jarosite Compounds

XRD data provide information on unit-cell dimensions and the degree of cation substitution in crystal structures and have been used to characterise jarosite subgroup minerals [17]. XRD can be used because variations in unit-cell dimensions are caused by differences between the ionic radii of elements contained in end members of the jarosite subgroup [18]. Therefore, unit-cell variations can be used to estimate the elemental ratios in solid solution between end members, that is, the extent of element substitutions [17,19]. Peak positions in XRD diffractograms can be used to determine unit-cell edge lengths, with shifts in XRD peak positions used to deduce structural incorporation of substituting cations in isomorphous minerals. The substitution of a smaller cation leads to a smaller unit cell, as indicated by shifts in all peaks towards higher 2 θ angles. Theoretically, the unit-cell edge lengths of mixed phases (solid solution) should lie in a straight line between those of two end members, according to Vegard's rule.

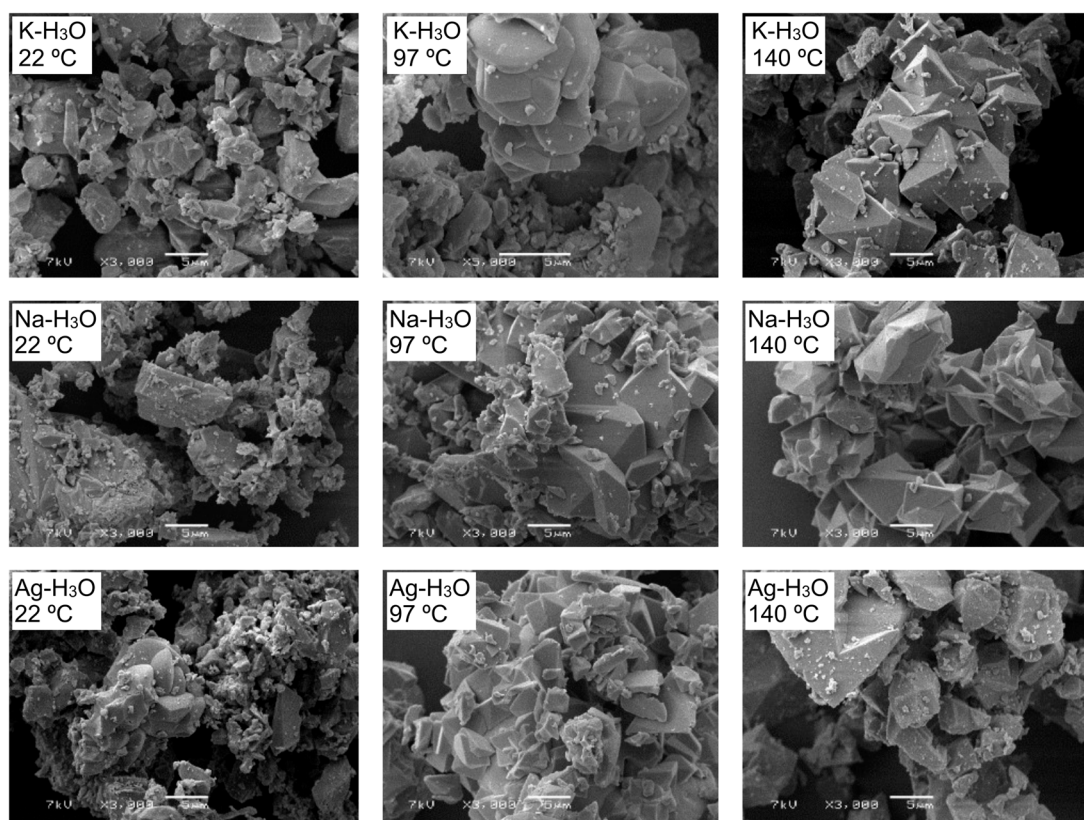


Figure 2. Photomicrographs of end-member K-H₃O, Na-H₃O and Ag-H₃O synthesised at 22 °C, 97 °C and 140 °C.

Jarosite phases were identified in all the synthesised samples using the X'Menu software. These synthetic jarosite phases were all consistent with the cations (K, Na and/or Ag) that were present in the starting solutions. No impurities were detected in the samples listed in Table 2. Representative examples of XRD diffractograms of the samples are shown in Figure 3.

The issue of changes in peak positions with cation substitution relates to mineral identification using JCPDS patterns because these patterns are based on minerals that are not necessarily end-member jarosite subgroup phases—for example, the JCPDS pattern 25-1327 of argentojarosite represents data for synthesised products reported by May et al. [7], for which the chemical formula is $\text{Ag}_{0.89-3}\text{Fe}_{2.93-3}(\text{SO}_4)_2(\text{OH})_6$, and JCPDS pattern 30-1203 of natrojarosite represents data for synthesised products reported by Dutrizac and Kaiman [8], for which the chemical formula is $\text{Na}_{0.82}\text{Fe}_{2.80}(\text{SO}_4)_2(\text{OH})_6$. This is problematic for the matching of standard patterns with peaks in synthesised jarosites of varying chemical compositions containing different proportions of cations.

The strongest intensity peaks of the JCPDS patterns of jarosite (22-0827) (3.08 Å), natrojarosite (30-1203) (3.06 Å), argentojarosite (25-1327) (3.062 Å) and hydronium jarosite (31-0650) (5.10 Å) are closely comparable with the main peaks of the synthesised K-Ag-H₃O and Na-Ag-H₃O jarosite products of this study. For example, the K-Ag-H₃O jarosite series of samples JS22, JS24, JS26, JS28 and JS30, which has declining K content and increasing Ag content, has the strongest peaks of 3.090 Å, 3.069 Å, 3.070 Å, 3.045 Å and 3.061 Å, respectively, which are consistent with the changing A-site occupation. In addition, Na-H₃O, the strongest peak of sample JS32, is at 5.066 Å, which is consistent with the strongest peak (5.10 Å) of hydronium jarosite (31-0650), rather than the strongest peak (3.06 Å) of natrojarosite (30-1203), and so are also consistent with the high proportion of H₃O in the samples indicated by the calculation of the mineral formula (Table 2).

Table 2. Starting solutions, site occupancy and XRD peaks of synthetic K-Ag-H₃O and Na-Ag-H₃O jarosite compounds. Peak shifts should be most pronounced of *c* parameters, which are indicated by hkl indices of 003 and 006 peaks.

Sample	Starting Solution	Type	Na	K	Ag	H ₃ O	Fe	Formula	hkl 003	hkl 006
K-Ag-H ₃ O-jarosite compounds										
Solutions containing 0.51 M Fe ₂ (SO ₄) ₃ ·5H ₂ O heated at 97 °C and products dried at 110 °C										
JS22	0.22 M K, 0.00 M Ag	K-H ₃ O	0.00	0.64	0.00	0.36	2.59	K _{0.64} (H ₃ O) _{0.36} Fe _{2.59} (H ₂ O) _{1.23} (OH) _{4.77} (SO ₄) ₂	5.721	2.853
JS24	0.165 M K, 0.055 M Ag	K-Ag-H ₃ O	0.00	0.53	0.15	0.32	2.62	K _{0.53} Ag _{0.15} (H ₃ O) _{0.32} Fe _{2.62} (H ₂ O) _{1.14} (OH) _{4.86} (SO ₄) ₂	5.629	2.824
JS26	0.11 M K, 0.11 M Ag	K-Ag-H ₃ O	0.00	0.44	0.25	0.31	2.74	K _{0.44} Ag _{0.25} (H ₃ O) _{0.31} Fe _{2.74} (H ₂ O) _{0.78} (OH) _{5.22} (SO ₄) ₂	5.606	2.809
JS28	0.055 M K, 0.165 M Ag	Ag-K-H ₃ O	0.00	0.27	0.56	0.17	2.57	K _{0.27} Ag _{0.56} (H ₃ O) _{0.17} Fe _{2.57} (H ₂ O) _{1.29} (OH) _{4.71} (SO ₄) ₂	5.519	2.774
JS30	0.00 M K, 0.22 M Ag	Ag-H ₃ O	0.00	0.00	1.00	0.00	2.62	Ag _{1.00} (H ₃ O) _{0.00} Fe _{2.62} (H ₂ O) _{1.14} (OH) _{4.86} (SO ₄) ₂	5.523	2.768
Solutions containing 0.15 M Fe ₂ (SO ₄) ₃ ·5H ₂ O heated at 140 °C and products dried at 110 °C										
JS55	0.12 M K, 0.00 M Ag	K-H ₃ O	0.00	0.57	0.00	0.43	2.75	K _{0.57} (H ₃ O) _{0.43} Fe _{2.75} (H ₂ O) _{0.75} (OH) _{5.25} (SO ₄) ₂	5.738	2.860
JS56	0.10 M K, 0.02 M Ag	K-Ag-H ₃ O	0.00	0.50	0.16	0.34	2.33	K _{0.50} Ag _{0.16} (H ₃ O) _{0.34} Fe _{2.33} (H ₂ O) _{2.01} (OH) _{3.99} (SO ₄) ₂	5.723	2.854
JS57	0.08 M K, 0.04 M Ag	K-Ag-H ₃ O	0.00	0.47	0.23	0.30	2.80	K _{0.47} Ag _{0.23} (H ₃ O) _{0.30} Fe _{2.80} (H ₂ O) _{0.60} (OH) _{5.40} (SO ₄) ₂	5.679	2.835
JS58	0.06 M K, 0.06 M Ag	K-Ag-H ₃ O	0.00	0.38	0.34	0.28	2.82	K _{0.38} Ag _{0.34} (H ₃ O) _{0.28} Fe _{2.82} (H ₂ O) _{0.54} (OH) _{5.46} (SO ₄) ₂	5.716	2.834
JS59	0.04 M K, 0.08 M Ag	K-Ag-H ₃ O	0.00	0.29	0.45	0.26	2.83	K _{0.29} Ag _{0.45} (H ₃ O) _{0.26} Fe _{2.83} (H ₂ O) _{0.51} (OH) _{5.49} (SO ₄) ₂	5.636	2.810
JS60	0.02 M K, 0.10 M Ag	Ag-K-H ₃ O	0.00	0.16	0.68	0.16	2.96	K _{0.16} Ag _{0.68} (H ₃ O) _{0.16} Fe _{2.96} (H ₂ O) _{0.12} (OH) _{5.88} (SO ₄) ₂	5.589	2.781
JS61	0.00 M K, 0.12 M Ag	Ag-H ₃ O	0.00	0.00	0.85	0.15	2.93	Ag _{0.85} (H ₃ O) _{0.15} Fe _{2.93} (H ₂ O) _{0.21} (OH) _{5.79} (SO ₄) ₂	5.543	2.767
Solutions containing 0.51 M Fe ₂ (SO ₄) ₃ ·5H ₂ O prepared at 22 °C and products air-dried at 22 °C										
JS73	0.22 M K, 0.00 M Ag	K-H ₃ O	0.00	0.78	0.00	0.22	2.40	K _{0.78} (H ₃ O) _{0.22} Fe _{2.40} (H ₂ O) _{1.80} (OH) _{4.20} (SO ₄) ₂	5.712	2.842
JS74	0.165 M K, 0.055 M Ag	K-Ag-H ₃ O	0.00	0.68	0.06	0.26	2.52	K _{0.68} Ag _{0.06} (H ₃ O) _{0.26} Fe _{2.52} (H ₂ O) _{1.44} (OH) _{4.56} (SO ₄) ₂	5.676	2.831
JS75	0.11 M K, 0.11 M Ag	K-Ag-H ₃ O	0.00	0.64	0.14	0.22	2.49	K _{0.64} Ag _{0.14} (H ₃ O) _{0.22} Fe _{2.49} (H ₂ O) _{1.53} (OH) _{4.47} (SO ₄) ₂	5.679	2.830
JS76	0.055 M K, 0.165 M Ag	K-Ag-H ₃ O	0.00	0.42	0.58	0.00	2.99	K _{0.42} Ag _{0.58} (H ₃ O) _{0.00} Fe _{2.99} (H ₂ O) _{0.03} (OH) _{5.97} (SO ₄) ₂	5.613	2.789
JS72	0.00 M M ^{+/2+} , 0.22 M Ag	Ag-H ₃ O	0.00	0.00	1.00	0.00	2.88	Ag _{1.00} (H ₃ O) _{0.00} Fe _{2.88} (H ₂ O) _{0.36} (OH) _{5.64} (SO ₄) ₂	5.740	2.855
Na-Ag-H ₃ O-jarosite compounds										
Solutions containing 0.51 M Fe ₂ (SO ₄) ₃ ·5H ₂ O heated at 97 °C and products dried at 110 °C										
JS32	0.22 M Na, 0.00 M Ag	Na-H ₃ O	0.02	0.00	0.00	0.98	2.87	Na _{0.02} (H ₃ O) _{0.98} Fe _{2.87} (H ₂ O) _{0.39} (OH) _{5.61} (SO ₄) ₂	5.580	2.791
JS34	0.165 M Na, 0.055 M Ag	Na-Ag-H ₃ O	0.47	0.00	0.43	0.10	2.97	Na _{0.47} Ag _{0.43} (H ₃ O) _{0.10} Fe _{2.97} (H ₂ O) _{0.09} (OH) _{5.91} (SO ₄) ₂	5.576	2.773
JS36	0.11 M Na, 0.11 M Ag	Ag-Na-H ₃ O	0.03	0.00	0.61	0.36	2.83	Na _{0.03} Ag _{0.61} (H ₃ O) _{0.36} Fe _{2.83} (H ₂ O) _{0.51} (OH) _{5.40} (SO ₄) ₂	5.568	2.778
JS38	0.055 M Na, 0.165 M Ag	Ag-Na-H ₃ O	0.04	0.00	0.61	0.35	2.59	Na _{0.04} Ag _{0.61} (H ₃ O) _{0.35} Fe _{2.59} (H ₂ O) _{1.23} (OH) _{4.77} (SO ₄) ₂	5.538	2.772
JS30	0.00 M Na, 0.22 M Ag	Ag-H ₃ O	0.00	0.00	1.00	0.00	2.62	Ag _{1.00} (H ₃ O) _{0.00} Fe _{2.62} (H ₂ O) _{1.14} (OH) _{4.86} (SO ₄) ₂	5.523	2.768
Solutions containing 0.15 M Fe ₂ (SO ₄) ₃ ·5H ₂ O heated at 140 °C and products dried at 110 °C										
JS49	0.12 M Na, 0.00 M Ag	Na-H ₃ O	0.47	0.00	0.00	0.53	2.64	Na _{0.47} (H ₃ O) _{0.53} Fe _{2.64} (H ₂ O) _{0.39} (OH) _{5.61} (SO ₄) ₂	5.597	2.801
JS50	0.10 M Na, 0.02 M Ag	Ag-Na-H ₃ O	0.16	0.00	0.23	0.61	3.04	Na _{0.16} Ag _{0.23} (H ₃ O) _{0.61} Fe ₃ (OH) ₆ (SO ₄) ₂	5.613	2.800
JS51	0.08 M Na, 0.04 M Ag	Ag-Na-H ₃ O	0.22	0.00	0.38	0.40	2.90	Na _{0.22} Ag _{0.38} (H ₃ O) _{0.40} Fe _{2.90} (H ₂ O) _{0.30} (OH) _{5.70} (SO ₄) ₂	5.603	2.778
JS52	0.06 M Na, 0.06 M Ag	Ag-Na-H ₃ O	0.17	0.00	0.45	0.38	2.93	Na _{0.17} Ag _{0.45} (H ₃ O) _{0.38} Fe _{2.93} (H ₂ O) _{0.21} (OH) _{5.79} (SO ₄) ₂	5.564	2.773
JS53	0.04 M Na, 0.08 M Ag	Ag-Na-H ₃ O	0.06	0.00	0.57	0.37	2.98	Na _{0.06} Ag _{0.57} (H ₃ O) _{0.37} Fe _{2.98} (H ₂ O) _{0.06} (OH) _{5.94} (SO ₄) ₂	5.559	2.777
JS54	0.02 M Na, 0.10 M Ag	Ag-Na-H ₃ O	0.04	0.00	0.66	0.30	2.98	Na _{0.04} Ag _{0.66} (H ₃ O) _{0.30} Fe _{2.98} (H ₂ O) _{0.06} (OH) _{5.94} (SO ₄) ₂	5.531	2.768
JS61	0.00 M Na, 0.12 M Ag	Ag-H ₃ O	0.00	0.00	0.85	0.15	2.93	Ag _{0.85} (H ₃ O) _{0.15} Fe _{2.93} (H ₂ O) _{0.21} (OH) _{5.79} (SO ₄) ₂	5.543	2.767

Table 2. *Cont.*[illegible]

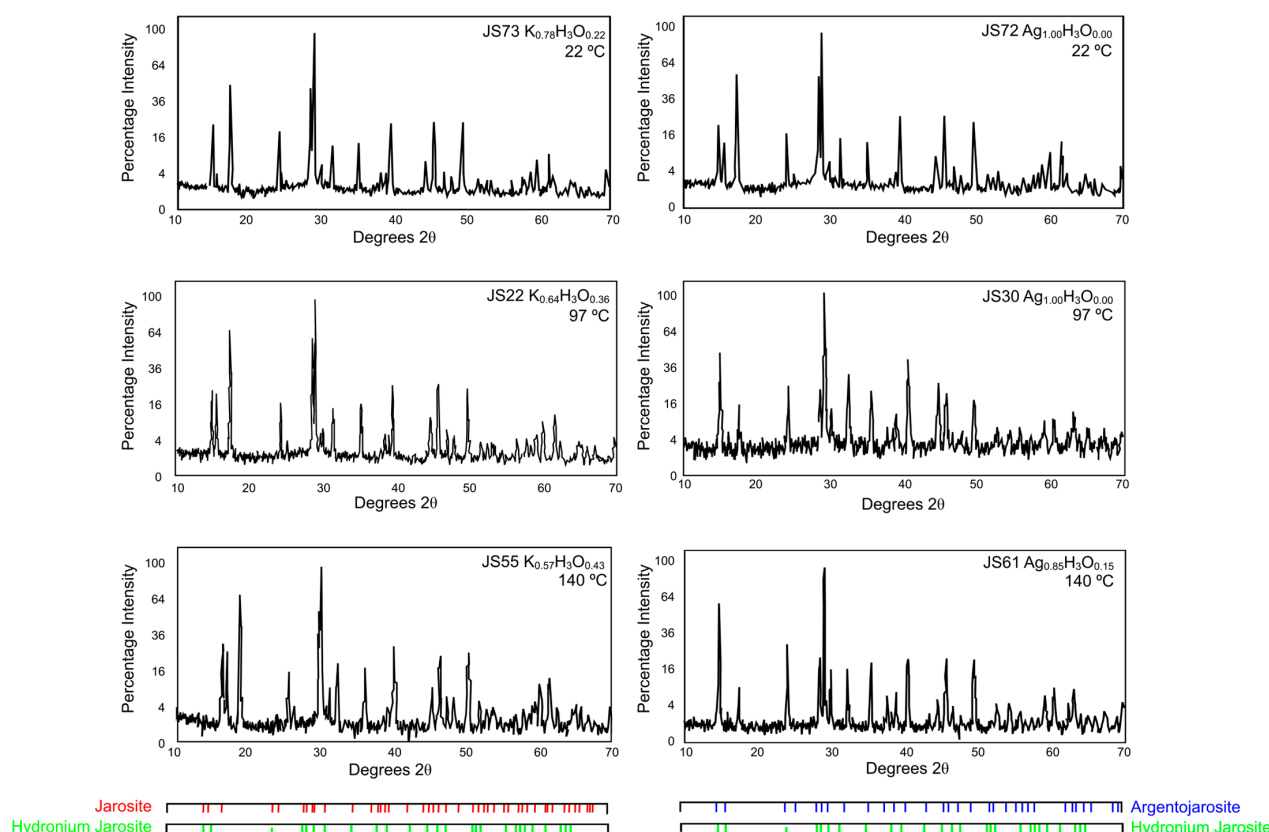


Figure 3. XRD diffractograms of synthetic end-member K-Ag-H₃O jarosite compounds at 22 °C, 97 °C and 140 °C.

The differences between the peak positions of the 003 and 006 (hkl) reflections (2θ degree angles) of jarosite, natrojarosite, hydroniumjarosite and mixtures of these end members are shown on X-ray diffractograms, and these results from the respective *c*-axis dimensions of the unit cells have been compared [3]. In theory, these *c*-axis parameters should vary according to the proportions of cations with different ionic radii occupying the *A* site. Table 2 lists the different positions (d-values) of the 003 and 006 reflections of the K-Ag-H₃O and Na-Ag-H₃O jarosite samples. In 12-fold coordination, the ionic radius of Na⁺ is 1.39 Å and K⁺ is 1.64 Å [20], that of Ag⁺ is 1.48 Å [21] and that of H₃O⁺ is 1.52 Å [5]. However, Groat et al. [22], in a study of the refined crystal structure of end-member argentojarosite, reported that Ag⁺ had an ionic radius of 1.35–1.36 Å, which was closer to 9-fold coordination than to 12-fold coordination, for which the predicted ionic radius was 1.48–1.56 Å.

The positions of the 003 and 006 reflections of jarosite (22-0827), natrojarosite (30-1203), argentojarosite (25-1327) and hydronium jarosite (31-0650) are closely comparable with those of the K, Na and Ag jarosite analogues synthesised in this study (Table 2). The positions of the 003 and 006 reflections in samples JS22–JS30 (the series of K-Ag-H₃O jarosite compounds synthesised at 97 °C), for example, show generally declining d-spacing values from 5.721 Å and 2.853 Å, respectively; for the jarosite product (JS22) containing K-H₃O only to 5.523 Å and 2.768 Å, respectively; and for the jarosite product (JS30) containing Ag-H₃O only. These results are consistent with the smaller radius of the Ag⁺ cation compared with K⁺ in 12-fold coordination. The other series of K-Ag jarosite analogues—JS55–JS61 (synthesised at 140 °C) and JS72–JS76 (synthesised at 22 °C)—show similar generally declining trends of 003 and 006 reflection d-spacings. However, the sample showing a significant deviation from this trend is JS72, a jarosite product containing Ag-H₃O only, which has unexplained anomalously large d-spacings for 003 and 006 reflections of 5.74 Å and 2.855 Å, respectively.

The Na-Ag jarosite analogues in sample series JS30–JS38 (synthesised at 97 °C) show a generally declining trend of *d*-values for the 003 and 006 reflections from 5.58 Å and 2.791 Å, respectively; in the product with Na-H₃O only in the *A* site to 5.523 Å and 2.768 Å, respectively; and in the product with Ag-H₃O only in the *A* site. These results are consistent with the Ag⁺ cation having a smaller radius than Na⁺ and, therefore, being in 9-fold coordination. The Na-Ag jarosite analogues in sample series JS71 and JS85–JS88 (synthesised at 140 °C) show a generally increasing trend of *d*-values for 003 and 006 reflections from 5.613 Å and 2.787 Å, respectively; in the product with Na-H₃O only in the *A* site to 5.627 Å and 2.792 Å, respectively; and in the product with Ag-H₃O only in the *A* site. These results are consistent with the Ag⁺ cation having a larger radius than Na⁺ and, therefore, being in 12-fold coordination. The Na-Ag jarosite analogue series JS49–JS54 and JS61 (synthesised at 140 °C) shows *d*-values increasing from the product with Na-H₃O only in the *A* site to the first intermediate product (lowest amount of Ag in the starting solution), then declining in the product series, and finally increasing again to the product with Ag-H₃O only in the *A* site. These results provide contradictory evidence on the cation sizes. The Na-Ag jarosite analogue series JS72 and JS77–JS80 (synthesised at 22 °C) has *d*-values that are anomalously high in samples JS72 and JS78, which complicates evidence of any pattern; however, there is a trend of increasing *d*-values in last three patterns in the series. Overall, this contradictory evidence from the *d*-values for 003 and 006 peaks about the respective sizes of the ionic radii of the Na and Ag cations and, therefore, whether Ag is in 9-fold or 12-fold coordination, may be the result of the presence of H₃O or vacancies in the *A* site.

3.3. Compositions of the Synthetic K-Ag-H₃O and Na-Ag-H₃O Compounds

Atomic percentages of the A-, B- and T-site elements were determined using the wet chemical data. The molecular compositions of the synthetic natrojarosites and jarosites, calculated using the modified formula of Kubisz [6] that sets the SO₄ in the structure to 2, are shown in Table 2. Almost all samples contained hydronium and had lower than expected Fe occupation at the B-site (i.e., less than the ideal of 3.00). The reason for the low Fe occupancy is as follows: If alkali ions are insufficient or depleted then hydronium ions (H₃O⁺) can substitute for them, resulting in a product with the general composition A_x(H₃O)_{1-x}Fe₃(SO₄)(OH)₆ (0 < *x* < 1). During this reaction, incomplete hydrolysis often results in substitution of H₂O for OH⁻, leading to an excess positive charge. Every three such disorders can result in the displacement of one Fe³⁺ ion, leading to Fe deficiency and the general composition for jarosite of K_x(H₃O)_{1-x}Fe_{3-y}(H₂O)_{3y}(OH)_{6-3y}(SO₄)₂, where *y* > 0 (and for natrojarosite of Na_x(H₃O)_{1-x}Fe_{3-y}(H₂O)_{3y}(OH)_{6-3y}(SO₄)₂).

The compositional results show a generally declining content of K and Na in the jarosite compounds with a declining alkali cation concentration in the starting solutions of each series with different initial synthesis temperatures (Table 2; Figure 4), suggesting that the starting-solution alkali content strongly influences the alkali content in the final product. Accompanying the trends of declining K and Na contents is a complementary trend of increasing Ag content as the concentration of Ag increases in the starting solutions (Table 2). The synthesised Na-H₃O- and K-H₃O-jarosites all incorporate Ag (Table 2; Figure 4). The degree of Ag incorporation increased with increasing synthesis temperature. A higher degree of Ag incorporation with the lowest initial concentration of Ag in the starting solution was achieved with the compounds synthesised at 140 °C compared to those synthesised at 97 °C and 22 °C. The Na-H₃O-jarosite compounds synthesised at 140 °C incorporated more Ag than the K-H₃O-jarosites for the same amounts of Ag in the starting solutions, as shown by the downward-facing curve in the former compared to the upward-facing curve in the latter in the molar Ag in Figure 4. This could be due to the preferential incorporation of K in jarosites compared to Ag and Na (Dutrizac and Jambor, 2000); K will be taken up preferentially to Ag, giving higher K:Ag ratios than analogous Na:Ag ratio in the Na-jarosites, which in turn could incorporate more Ag. Similar upward-facing curves are recorded for the K-H₃O-Ag-jarosite compounds synthesised at 97 °C and

22 °C, and for the Na-H₃O-Ag-jarosite compounds synthesised at 22 °C. By contrast, the Na-H₃O-Ag-jarosite compound curve is sigmoidal, due mainly to an anomalous molar Ag in the final solid value for sample JS36.

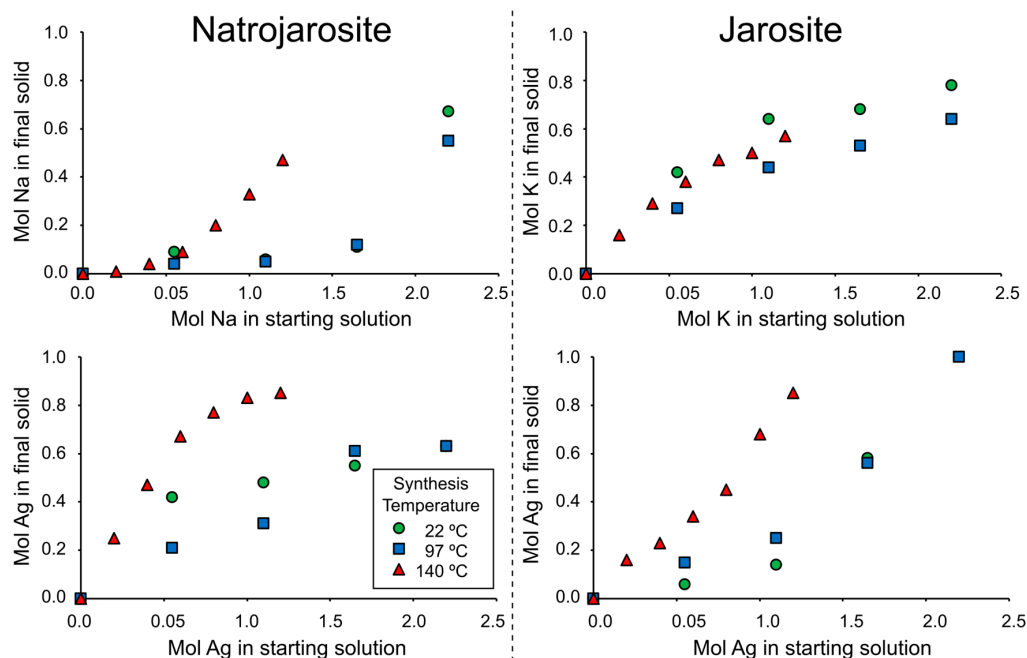


Figure 4. Comparison of moles of Na, K and Ag in the starting solutions with moles of Na, K and Ag in the final synthesised natrojarosite and jarosite solids.

The different series of compounds generally show good linear relationships between the content of the alkali and Ag cations in the products (Figure 5). For example, the K-Ag-H₃O jarosite series 55–61, synthesised at 140 °C, has an R^2 value of 0.989; series 22–30, synthesised at 97 °C, has an R^2 value of 0.996; and series 72–76, synthesised at 22 °C, has an R^2 value of 0.975 (Figure 5). The R^2 values of Na-Ag-H₃O series 49–54 and 61, synthesised at 140 °C, has an R^2 value of 0.999, but the other two Na-Ag-H₃O series have poorer linear relationships ($R^2 = 0.688$ for series 32–38 and 30, synthesised at 97 °C and $R^2 = 0.953$ for series 77–80 and 72, synthesised at 97 °C). The poorer R^2 values for the latter may be due to excess hydronium in the Na-Ag-H₃O jarosites made at these lower temperatures, or to an analytical error. The strong trends confirm that the Na-Ag-jarosite and K-Ag-jarosite solid solution series can form in the presence of H₃O, as previously shown by others for medium-to-high temperatures [9,14]. Our results also show that the solid solutions can exist at 22 °C.

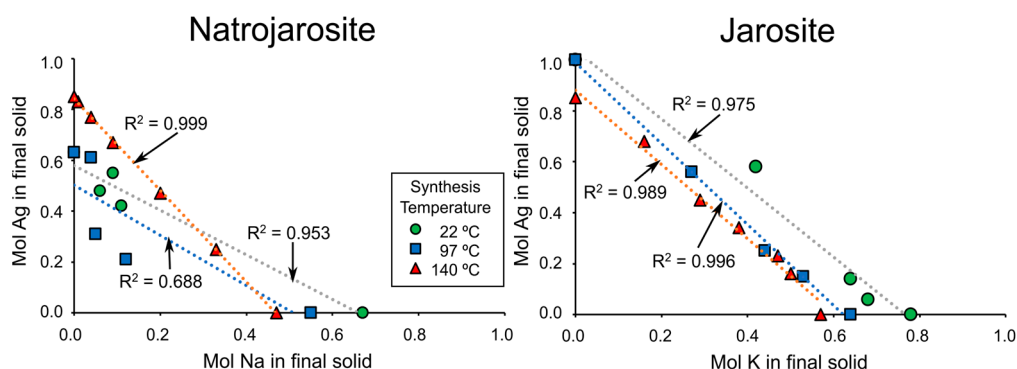


Figure 5. Moles Ag in the final synthesised natrojarosite and jarosite solids compared to moles Na and K in the final solids, respectively.

The K *A*-site contents of samples synthesised at 97 °C vary from 0.64 in sample JS22 (ideal site occupancy 1.0), from an initial solution concentration of 0.22 M K (and 0.00 M Ag) (and an Fe:K ratio in the starting solution of 4.64:1, so with excess Fe compared with the stoichiometric ratio of 3:1), to 0.27 in JS28, from a starting-solution K concentration of 0.055 M (and 0.165 M Ag) (Fe:K ratio 18.55:1). An increase in K content is seen moving from sample JS22 (0.64) to JS24 (0.53), in the series, sample JS06, in parallel with the decrease in the concentration of K in the starting solution of the latter, when Ag is first added to samples in the series. This phenomenon is also seen in samples JS55 and JS56 of series JS55-JS61, and in the Na-Ag-H₃O sample series synthesised at 22 °C and 140 °C, but not at 97 °C (Table 2).

Sample JS32, synthesised at 97 °C from an initial solution concentration of 0.22 M Na (0.00 M Ag) (Fe:Na ratio in 4.64:1), has an anomalously low Na content of 0.02. Similarly low Na contents are found in samples JS36 (Na content 0.03) and JS38 (Na content 0.04), both also synthesised at 97 °C, but from lower starting-solution Na concentrations of 0.11 M (and 0.11 M Ag) and 0.055 M (and 0.165 M Ag), respectively, and higher Fe:K ratios of 9.27:1 and 18.55:1, respectively, as well as in sample 80 (Na content 0.03), synthesised at 22 °C from a starting-solution Na concentration of 0.055 M (and 0.165 M Ag) (Fe:Na ratio 18.55:1). By contrast, sample JS34, synthesised at 97 °C from an initial solution concentration of 0.165 M Na (and 0.055 M Ag) (Fe:Na ratio 6.18:1), has an Na content of 0.47, respectively. The improved Na *A*-site content as a result of higher temperature of synthesis is indicated by the samples of series JS49-54, synthesised at 140 °C, which have high Na contents relative to their Fe:Na ratios in the starting solutions, compared with the products synthesised at 22 °C and 97 °C. This is likely to be a result of synthesis at 140 °C being above the boiling point of water, so limiting the amount of hydronium entering the *A* site.

Of the products synthesised at 97 °C, sample 30 has an Ag content of 1.00, from a starting-solution concentration of 0.22 M Ag with no alkali cations. The declining *A*-site occupancy of Ag in the products at a faster rate than the concentration of Ag in the synthesis solutions may be a result of the competition from the H₃O cation, which has a greater preference for this site than Ag in the jarosite crystal structure [1].

The *A*-site occupancy data (Table 2), which indicate higher temperatures of synthesis, generally have a tendency to increase the alkali and Ag occupancy of the *A* site of the products. The samples synthesised at 140 °C have relatively high K and Ag contents, and correspondingly lower H₃O contents, compared with the samples synthesised at lower temperatures, with regard to the cation concentrations in the starting solutions. Synthesised at 140 °C, sample 49 has an Na content of 0.47 and sample 50 has an Na content of 0.16, from starting-solution concentrations of 0.12 M (with no Ag) (Fe:Na ratio 2.5:1) and 0.10 M Na (and 0.02 M Ag) (Fe:Na ratio 3:1), respectively, which compare with 0.02 in sample 32, synthesised at 97 °C using 0.22 M Na (with no Ag) (Fe:Na ratio 4.64:1). Synthesised at 140 °C, sample 61 has an Ag content of 0.76, from an initial solution concentration of 0.12 M Ag (and no K or Na) (Fe:Ag ratio 2.5:1), which compares with Ag contents of 0.63 in sample 30, synthesised at 97 °C using 0.22 M Ag (and no alkali cations) (Fe:Ag ratio 4.64:1).

In the products synthesised at 22 °C, the K contents are higher than those synthesised at 97 °C. The products synthesised at 22 °C have lower Na contents compared with those synthesised at 97 °C; for example, sample JS78 has an Na content of 0.09 compared to 0.47 in sample JS34. The Ag-H₃O jarosites synthesised at 22 °C and 97 °C have similar Ag contents of 0.74 and 0.63, respectively. These are lower than the Ag content (0.76) in the product synthesised at 140 °C.

In the K-Ag jarosite compounds, the K content is consistently higher than the Ag content. The residual H₃O contents are high, and this may be a result of the excess Fe in the starting solutions, with the Fe:K ratio 4.64:1 compared with the stoichiometric jarosite ratio of 3:1. Some of the synthesised samples have high K contents compared to starting K concentrations in the starting solutions: examples are samples JS56 and JS57, which have K contents of 0.50 and 0.47, respectively; from starting solutions with K concentrations of 0.10 M and 0.08 M, respectively; and Fe:K ratios of 3:1 and 3.75:1, respectively. In the same

series, samples JS60 and JS61 have Ag contents of 0.68 and 0.85, respectively, from starting solutions with Ag concentrations of 0.10 M and 0.12 M, respectively. In almost all of the Na-Ag jarosite compounds, the Ag content is higher than the Na content.

The results suggest that, at all temperatures, the order of cation preference for occupancy of the A site in the synthesised compounds is $K > Na > H_3O > Ag$, which is consistent with the reported order of preference for incorporation into the A site of the jarosite structure [1]. The order is also consistent with Gibb's free energy data of -3309 kJ/mol, -3270 kJ/mol, -3247 kJ/mol and -2948 kJ/mol for jarosite, natrojarosite, hydronium-jarosite and argentojarosite, respectively [23].

3.4. The Raman Spectra

Jarosite exhibits spectral features as a result of the vibrational frequencies of the molecular bonds of sulfate groups, hydroxyl groups and metal-oxygen bonds, as well as lattice vibrations and iron excitations [24]. Sulfate tetrahedra in an aqueous solution possess T_d symmetry and vibrational frequencies which occur as a result of $\nu_1(SO_4^{2-})$ symmetric stretching, $\nu_2(SO_4^{2-})$ symmetric bending, $\nu_3(SO_4^{2-})$ asymmetric stretching and $\nu_4(SO_4^{2-})$ asymmetric bending, which are all Raman active [25,26]. The symmetric vibrational modes produce more intense bands compared with the other sulfate vibrations because of changes in polarizability [26]. Sulfates of jarosite have C_{3v} symmetry (monodentate, corner-sharing) and one ν_1 , one ν_2 , two ν_3 and two ν_4 frequencies are exhibited [24,26]. Fundamental frequencies and combinations and overtones are all observed [24]. In jarosites, other vibrational frequencies occur as a result of hydroxyl $\nu(OH)$ stretching, $\delta(OH)$ in-plane bending and $\gamma(OH)$ out-of-plane bending, as well as cation bonding in Fe-O and Fe-OH [25,27–29].

The Raman spectroscopic analyses of some of the synthetic jarosite compounds enabled the detected vibrational frequencies (wavenumbers, cm^{-1}) of the spectral peaks to be assigned to particular modes, which are shown in Table 3 and Figure 6. These assignments were made on the basis of comparison with reported frequencies and assigned modes [26–30] and comparison with detected peaks in samples of the RRUFF Project database of Raman spectra at the University of Arizona (see Table 3). For the synthesised K-Ag- H_3O jarosites of this study, the modes assigned to the detected ranges of vibrational frequencies (wavenumbers) are: Fe-O 221.1 – 228.4 cm^{-1} , 274.1 – 307.0 cm^{-1} , 353.3 – 371.9 cm^{-1} , 432.4 – 438.1 cm^{-1} ; $\nu_2(SO_4)$ 432.44 – 438.26 , 451.3 – 458.8 cm^{-1} ; Fe-OH 556.9 – 576.1 cm^{-1} ; $\nu_4(SO_4)$ 620.9 – 627.3 cm^{-1} ; $\nu_1(SO_4)$ 965.8 – 1013.6 cm^{-1} ; $\nu_3(SO_4)$ 1082.6 – 1110.1 cm^{-1} , 1120.2 – 1125.2 cm^{-1} , 1140.4 – 1166.8 cm^{-1} ; and $\nu(OH)$ 3378.5 – 3419.9 cm^{-1} (Table 4). For the synthesised Na-Ag jarosites, the vibrational frequencies and assigned modes are: Fe-O 224.6 – 228.4 cm^{-1} , 296.0 – 309.8 cm^{-1} , 358.9 – 371.9 cm^{-1} , 435.9 – 441.4 cm^{-1} ; $\nu_2(SO_4)$ 435.87 – 441.41 , 450.7 – 458.8 cm^{-1} ; Fe-OH 555.4 – 570.6 cm^{-1} ; $\nu_4(SO_4)$ 621.8 – 625.8 cm^{-1} ; $\nu_1(SO_4)$ 966.6 – 1016.2 cm^{-1} ; $\nu_3(SO_4)$ 1088.0 – 1114.3 cm^{-1} , 1122.2 – 1125.2 cm^{-1} , 1140.4 – 1165.3 cm^{-1} ; and $\nu(OH)$ 3378.5 – 3417.2 cm^{-1} (Table 5).

Table 3. Reported Raman frequencies (wavenumbers, cm^{-1}) and mode assignments in synthetic jarosite compound end members, and in jarosite-family compounds reported in other studies. Key: ¹ = [27]; ² = [25]; ³ = [29] [$\text{Na}_{0.53}(\text{H}_3\text{O})_{0.47}\text{Fe}_{1.79}(\text{OH})_6(\text{SO}_4)_2$]; ⁴ = [28] (natural jarosite); ⁵ = RRUFF project R060113; ⁶ = RRUFF project R070493; ⁷ = RRUFF project R050289; ⁸ = RRUFF project R050471; ⁹ = RRUFF project 060097; ¹⁰ = RRUFF project 060098. s = strong; w = weak; sh = shoulder; b = broad; sp = sharp. † = http://www.sci.qut.edu.au/sci_schps.html (accessed on 14 February 2016); RRUFF Project (integrated database of Raman spectra, XRD and chemistry data at the University of Arizona): <http://rruff.info/jarosite/display=default/> (accessed on 14 February 2016).

Mode	JS22	K ¹	K ²	K ⁵	K ⁶	JS32	Na ¹	Na ²	Na ³	Na ⁷	Na ⁸	JS30	Ag ²	Ag ⁴	Ag ⁹	Ag ¹⁰	H ₃ O ¹	H ₃ O ⁴					
ν OH	3411.7			3410.67 s	3412.36 s	3417.2					3401.95 s	3393.7 3378.5 w		3440.3				3452.0					
ν OH						3408.9								3399				3394	3388.85 s	3394.2	3380.52 s	3384.38 s	3410.9
ν OH						3399.2								3368						3371.6			3383.2
ν OH																							3372.0
ν OH																							
Unassigned	3077.7 w																						
Unassigned																							
Unassigned				2006.74 w	2012.29 w						2005.74 w				2215.73 w								
Unassigned				1688.55 w	1692.17 w						1672.52 w				2017.10 w								
Unassigned											1679.83 w				1679.62 w								
$\nu_3(\text{SO}_4^{2-})$	1158.4	1161	1153.33	1154.36	1159.91 s	1165.3	1160	1154.24 w	1152 w	1153.76	1155.29	1163.9	1160.58 w	1153.6	1157	1157	1163	1154.3					
$\nu_3(\text{SO}_4^{2-})$						1159.7						1140.4											
$\nu_3(\text{SO}_4^{2-})$	1125.2																						
$\nu_3(\text{SO}_4^{2-})$	1110.1	1112	1102.63 s	1102.29 s	1109.77 s	1108.7	1114	1112.59	1105	1109.41 s	1105.15 s	1110.1	1107.16	1104.5	1110.72 s	1108.79	1099	1102.9					
$\nu_3(\text{SO}_4^{2-})$	1104.5																						
$\nu_3(\text{SO}_4^{2-})$																							
$\nu_1(\text{SO}_4^{2-})$	1013.5	1015	1006.67	1009.73 s	1013.35	1013.5	1014	1012.10	1007	1012.98 s	1010.65	1088	1012.10	1011	1016.22 s	1016.22	1011	1007.3					
$\nu_1(\text{SO}_4^{2-})$	1009.3																						
$\nu_1(\text{SO}_4^{2-})$																							
†										974.41 sh		972.12			975.73 w								
Unassigned											840.95 b												
$\nu_4(\text{SO}_4^{2-})$						652								648.9				642.6					
$\nu_4(\text{SO}_4^{2-})$	627.16	625	624.61 s	625.96	631.51	625.78	627	624.61 sp	617 sp	625.36 s	623.03	624.4	622.80 sp	627.6	626.67 s	624.75	619	624.3					
$\nu_4(\text{SO}_4^{2-})$														621.0									
$\nu_4(\text{SO}_4^{2-})$														614.2									
γ OH		560	576.63 w	573.89	591.01 w	570.59	571	570.29 w	559 w	567.51 w	563.25	592.67	573.91 w		576.53 w	578.46 w	563	576.4					
O-Fe						563.69								562.7									
Fe-OH														558.5									
O-Fe	573.35											562.31					530	554.7					
$\nu_2(\text{SO}_4^{2-})$																							
$\nu_2(\text{SO}_4^{2-})$	456.06		453.50					450.78 sh				458.82		476.9				465.7					
$\nu_2(\text{SO}_4^{2-})$		442			444.54 s		445		445 sh	444.09 s	441.76 s		448.97 sh	440.6	445.40 s	445.40 s		453.4					
O-Fe	432.6		434.49 s	436.97 s		439.5		444.44 s	437 s			438.12	441.73 s					433.6					
O-Fe							406					371.89											
O-Fe	363.61		357.53 w	354.05		364.99	365	367.49 w	357 w	365.02 w	356.90 w	360.85	362.96 w		368.26 w		382						
O-Fe	302.9		301.40	300.05	303.67 w	309.79	303					307.04	305.93 sp		308.48 s	310.41							
O-Fe						296	295	298.68	288	295.59	299.05												
O-Fe	228.38		223.54 s	222.91 s	230.39 s	228.38	228	227.16	220	224.24 s	219.98 s	227	228.07	224.8	229.41 s	227.48		224.1					
Unassigned															188.91 w								
Unassigned					147.47 w		142			139.39 w	140.91				142.63 w	142.63 sw							
Unassigned																	110						

Table 4. Raman frequencies (wavenumber, cm^{-1}) and mode assignment for synthetic K-Ag- H_3O jarosite compounds. Key: B-O * = B-O (or OH-O, [28]); † = similar peak and assignment reported at http://www.sci.qut.edu.au/sci_schps.html (accessed on 14 February 2016); # assigned to $\delta(\text{H}_2\text{O})$ in the mid-IR study of synthetic K-jarosite in Bishop and Murad [24]; s = strong; w = weak; sh = shoulder; b = broad; sp = sharp.

Mode	JS22	JS73	JS55	JS24	JS74	JS26	JS75	JS28	JS76	JS56	JS57	JS58	JS59	JS60	JS30	JS72	JS61
Formula by chemistry	$\text{K}_{0.64}\text{H}_3\text{O}_{0.36}$	$\text{K}_{0.78}\text{H}_3\text{O}_{0.22}$	$\text{K}_{0.57}\text{H}_3\text{O}_{0.43}$	$\text{K}_{0.53}\text{Ag}_{0.15}\text{H}_3\text{O}_{0.32}$	$\text{K}_{0.68}\text{Ag}_{0.06}\text{H}_3\text{O}_{0.26}$	$\text{K}_{0.44}\text{Ag}_{0.25}\text{H}_3\text{O}_{0.31}$	$\text{K}_{0.64}\text{Ag}_{0.14}\text{H}_3\text{O}_{0.22}$	$\text{K}_{0.27}\text{Ag}_{0.56}\text{H}_3\text{O}_{0.17}$	$\text{K}_{0.42}\text{Ag}_{0.58}\text{H}_3\text{O}_{0.00}$	$\text{K}_{0.50}\text{Ag}_{0.16}\text{H}_3\text{O}_{0.34}$	$\text{K}_{0.47}\text{Ag}_{0.23}\text{H}_3\text{O}_{0.30}$	$\text{K}_{0.38}\text{Ag}_{0.34}\text{H}_3\text{O}_{0.28}$	$\text{K}_{0.29}\text{Ag}_{0.45}\text{H}_3\text{O}_{0.26}$	$\text{K}_{0.16}\text{Ag}_{0.68}\text{H}_3\text{O}_{0.16}$	$\text{Ag}_{1.00}\text{H}_3\text{O}_{0.00}$	$\text{Ag}_{1.00}\text{H}_3\text{O}_{0.00}$	$\text{Ag}_{0.85}\text{H}_3\text{O}_{0.15}$
Temp of Formation	97 °C	22 °C	140 °C	97 °C	22 °C	97 °C	22 °C	97 °C	22 °C	140 °C	140 °C	140 °C	140 °C	140 °C	97 °C	22 °C	140 °C
Temp of drying	110 °C	22 °C	110 °C	110 °C	22 °C	110 °C	22 °C	110 °C	22 °C	110 °C	110 °C	110 °C	110 °C	110 °C	110 °C	22 °C	110 °C
Unassigned			3586.4 w	3595.3 w	3586.4 w	3586.37 w			3592.4 w	3584.1 w	3585.2 w	3586.4 w	3581.8 w	3585.2		2592.4 s	3584.1 w
νOH								3417.3									
νOH	3411.7	3414.7	3412.08		3413.26		3410.01	3410.4	3411.18	3416.78	3408.5 s						
νOH				3407.6		3406.19		3407.6				3403.84					
νOH								3399.3									
νOH								3395.2					3397.95				
νOH														3384.97	3393.7	3373.43	3384.97
Unassigned								3123.4							3378.5		
Unassigned	3077.7 w	3080.1 w	3077.3 s	3075.1 s	3078.5 s	3077.3 s	3078.8 w		3077.6 s	3079.8 w	3078.5 s	3078.5 s	3078.5 s	3078.5 s		3080.1 s	3078.5 s
Unassigned											2762.5 w					2760.2	
Unassigned			2578.8 w		2576.2 w	2573.6 w			2577.8 w		2577.5 w	2477.5 w		2576.2 w		2580.5	2574.9 w
Unassigned		2409.88	2409.55		2410.9	2409.55			2413.92		2412.2 s	2408.21	2409.55	2410.9		2413.92	2408.21
Unassigned			2292.76		2294.13	2296.87			2295.83		2292.76					2299.93	
Unassigned			2206.08		2204.69	2206.08			2205.02	2207.46	2206.08	2204.69	2207.46	2203.31		2207.79	2204.69
Unassigned			2167.24		2165.85	2167.24	2165.85		2167.57	2167.24	2165.85	2165.85	2165.85	2165.85		2167.57	2165.85
Unassigned		2167.57	2103.01		2104.42	2104.42	2103.01		2104.75	2103.01	2103.01	2103.01	2103.01	2103.01		2104.75	2104.42
Unassigned		2103.35	2008.52							2007.1	2012.77	2014.19	2015.61	2012.77			2011.36
Unassigned																	
$2\nu_3(\text{SO}_4^{2-})/\delta\text{OH}$ #		1681.61	1682.74		1690.12		1690.48			1682.74	1679.78	1673.87	1672.39	1676.83			1667.95
$2\nu_3(\text{SO}_4^{2-})/\delta\text{OH}$			1404.72 s														
HOH																1232.12	
$\nu_3(\text{SO}_4^{2-})$				1162.6											1163.9		
$\nu_3(\text{SO}_4^{2-})$																	
$\nu_3(\text{SO}_4^{2-})$	1158.4	1158.46	1154.93		1154.93	1159.66	1156.88	1153	1158.46	1156.51	1156.51	1156.51	1156.51	1156.51			1156.51
$\nu_3(\text{SO}_4^{2-})$															1140.4		
$\nu_3(\text{SO}_4^{2-})$	1125.2		1123.38	1122.6	1123.38	1121.8	1121.8		1122.18		1121.8	1121.8		1120.22		1122.18	
$\nu_3(\text{SO}_4^{2-})$	1110.1							1108.8							1110.1		
$\nu_3(\text{SO}_4^{2-})$	1104.5	1103.18	1101.22	1106.1	1102.1	1104.39	1104.77		1104.77	1101.22	1102.81	1101.22	1101.22	1104.39		1104.77	1104.39
$\nu_3(\text{SO}_4^{2-})$				1100.5					1082.56								
$\nu_1(\text{SO}_4^{2-})$	1013.5			1013.6				1012.2							1088.		
$\nu_1(\text{SO}_4^{2-})$	1009.3	1007.58	1007.2	1006.7	1007.2	1008.8	1009.18	1009.5	1009.18	1007.2	1008.8	1008.8	1008.8	1010.4		1012.39	1012
$\nu_1(\text{SO}_4^{2-})^\dagger$								972.26	965.82							972.12	969.04
$\nu_4(\text{SO}_4^{2-})$	627.16			627.3													
$\nu_4(\text{SO}_4^{2-})$		624.21	623.81		623.81	623.81	624.21	623.16	620.85	623.81	623.81	622.13	622.13	622.13	624.4	622.53	622.13

Table 4. Cont.

Mode	JS22	JS73	JS55	JS24	JS74	JS26	JS75	JS28	JS76	JS56	JS57	JS58	JS59	JS60	JS30	JS72	JS61
Unassigned									592.32						592.67		
B-OH	573.35	572.12	570.04	572.11	573.41		572.12		570.44								
B-OH						564.98		561.07		566.66	564.98	563.29	561.6	563.29	562.31	562.01	559.92
B-OH																	
$\nu_2(\text{SO}_4^{2-})$	456.06	453.27	452.96		454.67	451.26		452.06	456.79	451.26	451.26				458.82		
$\nu_2(\text{SO}_4^{2-})$	432.6	432.85	432.44	438.26	432.44	432.44	432.85	435.5	434.56	430.73	432.44	434.16	434.16	437.58	438.12	437.99	437.58
B-O															371.89		
B-O	363.61	357.21	353.34		356.8	356.8		358.23	360.66	353.34	355.07	353.34	356.8	358.52	360.85	362.39	360.25
B-O	302.9	300.05		304.28	303.04	301.37	301.7	301.79	304.42	301.79		301.37	301.37	303.11	304.85	307.04	305.26
B-O			299.64								299.64						
B-O									274.06								
B-O *	228.38	223.27	222.85	227	223.01	224.6	225.8	225.02	225.77	226.77	222.85	222.85	221.1	222.85	224.6	227	226.77
Unassigned		138.75	138.33			140.1		140.52		138.75	138.33	138.33	138.33	138.33	138.33		138.75

Table 5. Raman frequencies (wavenumber, cm^{-1}) and mode assignment for synthetic Na-Ag- H_3O jarosite compounds. Key: B-O * = B-O (or OH-O, Frost et al., 2006b); + = similar peak and assignment reported at http://www.sci.qut.edu.au/sci_schps.html (accessed on 14 February 2016); # assigned to $\delta(\text{H}_2\text{O})$ in the mid-IR study of synthetic K-jarosite in Bishop and Murad [24]; s = strong; w = weak; sh = shoulder; b = broad; sp = sharp.

Mode	JS32	JS49	JS34	JS78	JS36	JS38	JS80	JS50	JS51	JS52	JS53	JS54	JS30	JS72	JS61
Formula by chemistry	Na _{0.02} H ₃ O _{0.98}	Na _{0.47} H ₃ O _{0.53}	Na _{0.47} Ag _{0.43} H ₃ O _{0.10}	Na _{0.09} Ag _{0.61} H ₃ O _{0.30}	Na _{0.03} Ag _{0.61} H ₃ O _{0.36}	Na _{0.04} Ag _{0.61} H ₃ O _{0.35}	Na _{0.03} Ag _{0.68} H ₃ O _{0.29}	Na _{0.16} Ag _{0.23} H ₃ O _{0.61}	Na _{0.22} Ag _{0.38} H ₃ O _{0.40}	Na _{0.17} Ag _{0.45} H ₃ O _{0.38}	Na _{0.06} Ag _{0.57} H ₃ O _{0.37}	Na _{0.04} Ag _{0.66} H ₃ O _{0.30}	Ag _{0.63} H ₃ O _{0.37}	Ag _{0.74} H ₃ O _{0.26}	Ag _{0.76} H ₃ O _{0.24}
Temp of Formation	97 °C	140 °C	97 °C	22 °C	97 °C	97 °C	22 °C	140 °C	140 °C	140 °C	140 °C	140 °C	97 °C	22 °C	140 °C
Temp of drying	110 °C	110 °C	110 °C	22 °C	110 °C	110 °C	22 °C	110 °C	110 °C	110 °C	110 °C	110 °C	110 °C	22 °C	110 °C
Unassigned		3578.6 w	3578.3 w	3585.5 w					3586.6 w	3585.5 w	3585.5 w	3584.4 w		3592.4 s	3584.1 w
νOH	3417.2														
νOH	3408.9	3405.3						3401.76							
νOH	3399.2		3396.77						3398.23						
νOH			3392.05	3389.69	3393.8	3388.2	3388.79			3384.07	3382.89	3393.51	3393.7	3373.43	3384.97
νOH													3378.5 w		
Unassigned		3078.8	3076.1	3078.8	3082 w	3081.9 w	3078.8	3078.8 w	3078.8	3080.1	3077.6	3078.8 s		3080.1 s	3078.5 s
Unassigned												2752.5 w		2760.2	
Unassigned		2576.5 w							2581.8 w	2579.2 w	2583.1 w	2475.2 w		2580.5	2574.9 w
Unassigned		2409.88	2410.9						2411.22	2412.57	2408.53	2412.57		2413.92	2408.21
Unassigned									2295.83			2291.72		2299.93	
Unassigned		2206.41							2205.02	2207.79	2205.02	2206.41		2207.79	2204.69
Unassigned		2166.18	2167.24						2167.57	2166.18	2167.57	2167.57		2167.57	2165.85
Unassigned		2104.75	2103.01	2167.57			2167.57		2104.75	2103.35	2103.35	2103.35		2104.75	2104.42
Unassigned		2020.2		2103.35			2103.35	2015.95	2018.78	2014.53	2017.37	2013.11			2011.36
Unassigned															
Unassigned		1687.52	1673.87	1680.14			1681.61	1687.52	1678.66	1684.57	1680.14	1666.82			1667.95

Table 5. Cont.

Mode	JS32	JS49	JS34	JS78	JS36	JS38	JS80	JS50	JS51	JS52	JS53	JS54	JS30	JS72	JS61
$2\nu_3(\text{SO}_4^{2-}) /$															
2 δOH #															
HOH														1232.12	
$\nu_3(\text{SO}_4^{2-})$	1165.3					1163.9						1160.03	1163.9		
$\nu_3(\text{SO}_4^{2-})$	1159.7	1158.46	1158.08	1158.46	1159.9	1154.2	1156.88	1158.46	1158.46	1158.46	1158.46				1156.51
$\nu_3(\text{SO}_4^{2-})$													1140.4		
$\nu_3(\text{SO}_4^{2-})$			1123.38									1122.18		1122.18	
$\nu_3(\text{SO}_4^{2-})$	1108.7				1107.4	1110.1							1110.1		
$\nu_3(\text{SO}_4^{2-})$		1106.35	1105.97	1106.35			1106.35	1106.35	1106.35	1106.35	1106.35	1104.77		1104.77	1104.39
$\nu_3(\text{SO}_4^{2-})$													1088		
$\nu_3(\text{SO}_4^{2-})$	1013.5	1012.39	1012	1012.39	1012.2	1013.5	1012.39	1012.39	1012.39	1012.39	1012.39	1012.39	1013.5	1012.39	1012
$\nu_1(\text{SO}_4^{2-}) \dagger$						966.61							972.12	969.04	
$\nu_4(\text{SO}_4^{2-})$	652														
$\nu_4(\text{SO}_4^{2-})$	625.78	622.53	622.13	622.53	621.78	624.4	622.53	622.53	622.53	622.53	622.53	622.53	624.4	622.53	622.13
Unassigned													592.67		
B-OH	570.59														
B-OH	563.69	563.69		563.69	561.07	567.83	562.01	562.01	562.01	560.32	560.32		562.31	562.01	559.92
B-OH			558.23			558.17						558.63			
$\nu_2(\text{SO}_4^{2-})$													458.82		
$\nu_2(\text{SO}_4^{2-})$	439.5	437.99	435.87	439.7	436.88	438.12	437.99	437.99	436.28	437.99	437.99	437.99	438.12	437.99	437.58
B-O					366.51	366.37							371.89		
B-O	364.99	360.66	360.25	362.39		359.47	365.84	360.66	360.66	362.39	358.94	362.39	360.85	362.39	360.25
B-O	309.79	300.05	303.11	307	304.42	308.42	307	303.53	305.26	305.26	305.26	305.26	307.04	305.26	304.85
B-O	296														
B-O *	228.38	225.02	224.6	226.77	227.15	228.38	226.77	226.77	225.02	225.02	225.02	225.02	227	226.77	224.6
Unassigned		136.98	138.33	138.75			140.52	136.98	138.75	138.75	138.75	138.75		138.75	138.33

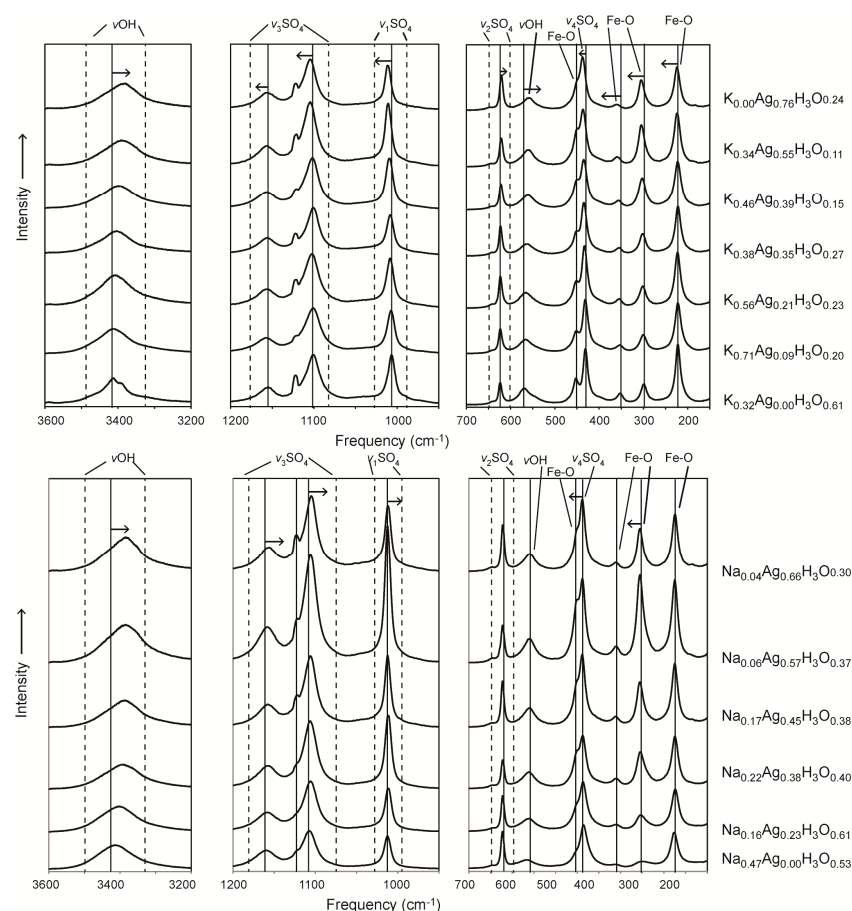


Figure 6. Raman spectra for K-Ag-H₃O and Na-Ag-H₃O compounds synthesised at 140 °C and dried at 110 °C.

The Raman spectra of the synthesised K-Ag and Na-Ag jarosites also contain bands that have not been reported in previous Raman studies (Tables 4 and 5). These include peaks at 3581.8–3595.3 cm^{−1} in K-Ag samples and 3578.3–3593.5 cm^{−1} in Na-Ag samples. Of these, the only strong band strength was in the Ag sample JS72 at 3592.4 cm^{−1}; in all the other samples, the band strengths were weak. These peaks have been assigned to a hydroxyl stretching mode, $\nu(\text{OH})$, or water stretching mode, $\nu(\text{H}_2\text{O})$, on the basis of evidence from other studies. Raman peaks at 3515 cm^{−1} were assigned to $\nu(\text{OH})$ in Sasaki et al. [25], whereas IR peaks at 3501 cm^{−1} were assigned to $\nu(\text{H}_2\text{O})$ in Powers et al. [31]. IR peaks at ~3550 cm^{−1} (medium band strength) in synthetic Na-jarosite and K-jarosite and ~3550 cm^{−1} (weak band strength) in natural jarosite were assigned to $\nu(\text{H}_2\text{O})$ in Bishop and Murad [24]. A study of the IR spectrum of K-jarosite reports a broad profile centred on 3356 cm^{−1} with overlapping bands of $\nu(\text{OH})$ (hydroxyl stretching) modes and adsorbed water extending from 3590 to 2600 cm^{−1}; however, Raman analysis does not show bands of adsorbed water [28]. IR spectral bands at ~3600 cm^{−1} have been assigned to $\nu(\text{OH})$ bands in the sulfates gypsum and ettringite [26].

Spectral bands were detected at 3075.1–3080.1 cm^{−1} in K-Ag samples and 3075.1–3082 cm^{−1} in Na-Ag samples. Strong band strengths were present in Ag-jarosite samples JS72 and JS61, and in K-Ag samples JS24, JS26, JS55, JS57, JS58, JS59, JS60, JS74 and JS76; medium strength peaks were present in Na-Ag samples JS34, JS49, JS51, JS52, JS53, JS78 and JS80, and all other peaks were weak. These peaks have been assigned to $\nu(\text{OH})$, on the basis of the IR study of K-jarosite by Frost et al. [28], reporting a broad profile centred on 3356 cm^{−1} with overlapping bands of $\nu(\text{OH})$ modes from 3590 to 2600 cm^{−1}. For the same reason, two further band ranges have been assigned to $\nu(\text{OH})$. The first are peaks at 2760.2–2762.5 cm^{−1} in K-Ag samples and 2752.5–2760.2 cm^{−1} in Na-Ag samples. Ag-jarosite sample JS72

has a medium-strength band at 2760.2 cm^{-1} ; all other bands in the range are weak. The second are peaks at $2573.6\text{--}2580.5\text{ cm}^{-1}$ in K-Ag samples and $2574.9\text{--}2583.1\text{ cm}^{-1}$ in Na-Ag samples. Again, only Ag-jarosite sample JS72 has a medium-strength band; all other bands in the range are weak.

Spectral bands were present at $1668.0\text{--}1690.5\text{ cm}^{-1}$ in K-Ag samples and $1598.4\text{--}1687.5\text{ cm}^{-1}$ in Na-Ag samples. These have been assigned to $2\nu_3(\text{SO}_4^{2-})/2\delta\text{OH}$, on the basis of reported IR bands at 1634 s cm^{-1} in synthetic K-jarosite and at 1639 s cm^{-1} in synthetic Na-jarosite and at 1630 cm^{-1} in natural K-jarosite, which were assigned to $\delta(\text{H}_2\text{O})$ (in-plane bending) [25]. In addition, RRUFF Project jarosite samples R060113 (K-jarosite), R070493 (K-jarosite), R050289 (Na-jarosite), R050471 (Na-jarosite) and 060097 (Ag-jarosite) show weak, broad peaks at $1672.5\text{--}1692.2\text{ cm}^{-1}$.

Raman frequency differences in vibrational modes with different A-site substitutions in the jarosite structure may be caused by the heaviness (atomic number) of the elements present [30]. These frequency differences may be due to differences in the bonding to the metal cations, thus revealing small but important structural differences with cation substitution, which may be due to the different electronic configurations of Ag (a transition metal) and K and Na (alkali metals) [30]. In some of the synthesised products in this study, the assigned vibrational modes of the K-H₃O-synthesised products have higher wavenumbers (cm^{-1}) than their Ag-H₃O equivalents, which is consistent with some reported modes but not with others [25,27,28,30]: compounds JS22 and JS30 (97°C), νOH (3411.7 and 3393.7), $\nu_3\text{SO}_4$ (lower reading, 1104.5 and 1088), $\nu_1\text{SO}_4$ (lower reading, 1009.3 and 972.12) and $\nu_4\text{SO}_4$ (627.16 and 624.4). Therefore, these results are not consistent with predicted stronger bonds for heavier elements [30]; this could be due to the contents of H₃O in the synthetic compounds produced in this study. In some other cases, the K-H₃O products have lower wavenumbers than their Ag-H₃O equivalents, thereby providing evidence of stronger bonds for Ag: compounds JS22 and JS30 (97°C), $\nu_3\text{SO}_4$ (upper reading, 1158.4 and 1163.9) and $\nu_2\text{SO}_4$ (432.6 and 438.12); compounds JS55 and JS61 (140°C), $\nu_3\text{SO}_4$ (1101.22 and 1104.39 ; 1154.93 and 1156.51), $\nu_1\text{SO}_4$ (1007.2 and 1012) and $\nu_2\text{SO}_4$ (432.44 and 437.58); and products JS73 and JS72 (22°C), $\nu_3\text{SO}_4$ (lower reading, 1103.18 and 1104.77), $\nu_1\text{SO}_4$ (1007.58 and 1012.39) and $\nu_2\text{SO}_4$ (432.85 and 437.99).

In all cases, the assigned modes of Ag-H₃O products do not have higher wavenumbers than their Na-H₃O equivalents, but some have the same wavenumbers, which is consistent with some reported modes but not with others (Tables 4 and 5) ([25,28] RRUFF projects 060097 and 060098). The Na-H₃O modes with higher wavenumbers than their Ag-H₃O equivalents are: compounds JS32 and JS30 (97°C), νOH (3399.2 and 3393.7), $\nu_3\text{SO}_4$ (1108.7 and 1088 ; 1165.3 and 1163.9), $\nu_4\text{SO}_4$ (625.78 and 624.4) and $\nu_2\text{SO}_4$ (439.5 and 438.12); compounds JS49 and JS61 (140°C), νOH (3405.3 and 3384.97) and $\nu_3\text{SO}_4$ (1106.35 and 1104.39 ; and 1158.46 and 1156.51); and compounds JS77 and JS72 (22°C), νOH (3401.76 and 3373.43), $\nu_3\text{SO}_4$ (1107.94 and 1104.77 ; 1156.88 and 1122.18), $\nu_4\text{SO}_4$ (624.21 and 622.53) and $\nu_2\text{SO}_4$ (441.41 and 437.99). Therefore, these results are also not consistent with the predicted stronger bonds for heavier elements [30], which again could be due to the H₃O incorporated in this study's synthetic compounds.

In many of the series of synthesised K-Ag-H₃O and Na-Ag-H₃O jarosite products, no clear trend is discernible in the wavenumbers of the assigned modes. The K-Ag-H₃O series in which trends may be observed are: JS22–JS30 (97°C), $\nu_4\text{SO}_4$ (decreasing cm^{-1}); JS55–JS61 (140°C), νOH (decreasing cm^{-1}), $\nu_3\text{SO}_4$ (increasing cm^{-1}) and $\nu_1\text{SO}_4$ (increasing cm^{-1}); and 72–76 (22°C), νOH (decreasing cm^{-1}), $\nu_1\text{SO}_4$ (increasing cm^{-1}) and $\nu_2\text{SO}_4$ (increasing cm^{-1}). The Na-Ag-H₃O series in which trends may be observed are: JS30–JS38 (97°C), $\nu_3\text{SO}_4$ (increasing cm^{-1} , except the Na-H₃O and Ag-H₃O products) and $\nu_2\text{SO}_4$ (increasing cm^{-1} , except the Na-H₃O product); JS49–JS54 and JS61 (140°C), νOH (decreasing cm^{-1}) and $\nu_3\text{SO}_4$ (decreasing cm^{-1}); and JS72 and JS77–80 (22°C), $\nu_2\text{SO}_4$ (decreasing cm^{-1}).

In the Fe-O modes, the K-Ag-synthesised products have lower ranges of frequencies than the Na-Ag products, which is not consistent with some reported modes ([28,29] RRUFF project R050471), but is with other reported modes ([25,30] RRUFF project R060113).

Therefore, these results provide contradictory evidence on any relationship between Fe-O bonding and A-site substitution. It is likely that there is a relationship; however, the lack of consistency with previous research suggests that products of different compositions were analysed compared to those in our study, or that the presence of hydronium in the solids affected the mode frequencies.

4. Conclusions

Jarosite compounds with the A site filled with K, Na, Ag and H₃O were synthesised at 22 °C, 97 °C and 140 °C, and these were characterised by XRD, SEM, chemical analysis and Raman spectroscopy. The jarosite and natrojarosite compounds all took up Ag, especially in the 140 °C synthesis. Silver is the least favoured, however, of K, Na and H₃O to occupy the A site in the synthesized compounds due to the lower stability it infers on the solids. Despite this, the compounds took up increasing amounts of Ag that correlated with the amounts of Ag in the starting solutions, despite high degrees of H₃O incorporation, especially in the lower temperature syntheses. The SEM, XRD and Raman characterisation methods were effective at distinguishing the different jarosite compounds, and the resultant database will be useful for predicting the capacity of jarosite family minerals for the uptake of Ag in natural and engineered environments.

Author Contributions: Conceptualization, K.A.H.-E. and P.F.C.; methodology, P.F.C., K.A.H.-E. and M.D.W.; formal analysis, P.F.C., K.A.H.-E. and M.D.W.; investigation, P.F.C., K.A.H.-E. and M.D.W.; resources, K.A.H.-E. and M.D.W.; data curation, K.A.H.-E.; writing—original draft preparation, P.F.C.; writing—review and editing, P.F.C., K.A.H.-E. and M.D.W.; visualization, P.F.C., K.A.H.-E. and M.D.W.; supervision, K.A.H.-E. and M.D.W.; project administration, K.A.H.-E.; funding acquisition, K.A.H.-E. All authors have read and agreed to the published version of the manuscript.

Funding: This research was funded by a postgraduate studentship to P.F. Cogram granted by Birkbeck, University of London.

Data Availability Statement: Data for this paper can be found in this article and at <https://eprints.bbk.ac.uk/id/eprint/40262/> (accessed on 2 February 2023).

Acknowledgments: This work was funded through a Birkbeck postgraduate research studentship to P.F. Cogram. We thank A. Beard for assistance with electron microprobe analysis, S. Hirons for help with XRD analysis, J. Davy for help with SEM analysis, P. Murphy and S. Crust for assistance with Raman analysis, G. Tarbuck for assistance with acid digestion and ICP-OES analysis, and A. Osborn for help with the synthesis of jarosite compounds.

Conflicts of Interest: The authors declare no conflict of interest. The funders had no role in the design of the study; in the collection, analyses, or interpretation of data; in the writing of the manuscript; or in the decision to publish the results.

References

1. Jambor, J.L. Nomenclature of the alunite supergroup. *Can. Mineral.* **1999**, *37*, 1323–1341.
2. Hawthorne, F.C.; Krivovichev, S.V.; Burns, P.C. Crystal chemistry of sulphate minerals. *Rev. Mineral. Geochem.* **2000**, *40*, 405–452. [\[CrossRef\]](#)
3. Desborough, G.A.; Smith, K.S.; Lowers, H.A.; Swayze, G.A.; Hammarstrom, J.M.; Diehl, S.F.; Leinz, R.W.; Driscoll, R.L. Mineralogical and chemical characteristics of some natural jarosites. *Geochim. Cosmochim. Acta* **2010**, *74*, 1041–1056. [\[CrossRef\]](#)
4. Majzlan, J.; Stevens, R.; Boerio-Goates, J.; Woodfield, B.F.; Navrotsky, A.; Burns, P.C.; Crawford, M.K.; Amos, T.G. Thermodynamic properties, low-temperature heat-capacity anomalies, and single-crystal X-ray refinement of hydronium jarosite, (H₃O)Fe₃(SO₄)₂(OH)₆. *Phys. Chem. Miner.* **2004**, *31*, 518–531. [\[CrossRef\]](#)
5. Basciano, L.C.; Peterson, R.C. Crystal chemistry of the natrojarosite–jarosite and natrojarosite–hydronium jarosite solid solution series: A synthetic study with full iron site occupancy. *Am. Mineral.* **2008**, *93*, 853–862. [\[CrossRef\]](#)
6. Kubisz, J. Studies on synthetic alkali-hydronium jarosites: I. Synthesis of jarosite and natrojarosite. *Mineral. Polonica* **1970**, *1*, 47–59.
7. May, A.; Sjöberg, J.J.; Baglin, E.G. Synthetic argentojarosite: Physical properties and thermal behaviour. *Am. Mineral.* **1973**, *58*, 936–941.
8. Dutrizac, J.E.; Kaiman, S. Synthesis and properties of jarosite-type compounds. *Can. Mineral.* **1976**, *14*, 151–158.

9. Dutrizac, J.E.; Jambor, J.L. Formation and characterization of argentojarosite and plumbojarosite and their relevance to metallurgical processing. In Proceedings of the Second International Congress on Applied Mineralogy in the Minerals Industry, Los Angeles, CA, USA, 22–25 February 1984; Park, W.D., Hausen, D.M., Hagni, R.D., Eds.; AIME: New York, NY, USA, 1984; pp. 507–530.
10. Dutrizac, J.E.; Jambor, J.L. The behavior of arsenic during jarosite precipitation: Arsenic precipitation at 97 degrees from sulfate or chloride media. *Can. Metall. Q.* **1987**, *26*, 91–101. [\[CrossRef\]](#)
11. Patino, F.; Salinas, E.; Cruells, M.; Roca, A. Alkaline decomposition cyanidation kinetics of argentian natrojarosite. *Hydrometallurgy* **1998**, *49*, 323–336. [\[CrossRef\]](#)
12. Calla-Choque, D.; Lapidus, G.T. Acid decomposition and silver leaching with thiourea and oxalate from an industrial jarosite sample. *Hydrometallurgy* **2020**, *192*, 105289. [\[CrossRef\]](#)
13. Islas, H.; Flores, M.U.; Juárez, J.C.; Reyes, M.; Blanco, A.; Gutiérrez, E.; Aguilar, J.; Nolasco, M.C.; Rodríguez, I.; Reyes, I.A. Silver leaching from jarosite-type compounds using cyanide and non-cyanide lixiviants: A kinetic approach. *Miner. Eng.* **2021**, *174*, 107250. [\[CrossRef\]](#)
14. Ildefonse, J.P.; Le Toullec, C.; Perrotel, V. About the synthetic lead–silver jarosite solid solution. In *Experimental Mineralogy and Geochemistry, International Symposium*; Nancy: San Francisco, CA, USA, 1986; pp. 72–73.
15. Anthony, J.W.; Bideaux, R.A.; Bladh, K.W.; Nichols, M.C. *Handbook of Mineralogy*; Mineralogical Society of America: Chantilly, VA, USA, 2003.
16. Gasharova, B.; Gottlicher, J.; Becker, U. Dissolution at the surface of jarosite: An in-situ AFM study. *Chem. Geol.* **2005**, *215*, 499–516. [\[CrossRef\]](#)
17. Desborough, G.A.; Smith, K.S.; Lowers, H.A.; Swayze, G.A.; Hammarstrom, J.M.; Diehl, S.F.; Driscoll, R.L.; Leinz, R.W. The use of synthetic jarosite as an analog for natural jarosite. In Proceedings of the Seventh International Conference on Acid Rock Drainage (ICARD 7), St Louis, MO, USA, 26–30 March 2006; pp. 458–475.
18. Brophy, G.P.; Sheridan, M.F. Sulphate studies IV: The jarosite-natrojarosite-hydronium jarosite solid solution series. *Am. Mineral.* **1965**, *50*, 1595–1607.
19. Papike, J.J.; Karner, J.M.; Shearer, C.K. Implications of Martian and terrestrial jarosite: A crystal chemical perspective. *Geochim. Cosmochim. Acta* **2006**, *70*, 1309–1321. [\[CrossRef\]](#)
20. Shannon, R.D. Revised effective radii and systematic studies of interatomic distances in halides and chalcogenides. *Acta Crystal.* **1976**, *A32*, 751–767. [\[CrossRef\]](#)
21. Dutrizac, J.E.; Jambor, J.L. Jarosites and their application in hydrometallurgy. *Rev. Mineral. Geochem.* **2000**, *40*, 405–452. [\[CrossRef\]](#)
22. Groat, L.A.; Jambor, J.L.; Pemberton, B.C. The crystal structure of argentojarosite, $\text{AgFe}_3(\text{SO}_4)_2(\text{OH})_6$. *Can. Mineral.* **2003**, *41*, 921–928. [\[CrossRef\]](#)
23. Gaboreau, S.; Vieillard, P. Prediction of Gibbs free energies of formation of minerals of the alunite supergroup. *Geochim. Cosmochim. Acta* **2004**, *68*, 3307–3316. [\[CrossRef\]](#)
24. Bishop, J.L.; Murad, E. The visible and infrared spectral properties of jarosite and alunite. *Am. Mineral.* **2005**, *90*, 1100–1107. [\[CrossRef\]](#)
25. Sasaki, K.; Tanaike, O.; Konno, H. Distinction of jarosite-group compounds by Raman spectroscopy. *Can. Mineral.* **1998**, *36*, 1225–1235.
26. Myneni, S.C.B. X-ray and vibrational spectroscopy of sulphate in earth materials. *Rev. Mineral. Geochem.* **2000**, *40*, 113–172. [\[CrossRef\]](#)
27. Serna, C.J.; Parada Cortina, C.; Garcia Ramos, J.V. Infrared and Raman study of alunite-jarosite compounds. *Spectrochim. Acta* **1986**, *42A*, 729–734. [\[CrossRef\]](#)
28. Frost, R.; Wills, R.-A.; Weier, M.; Martens, W. A Raman spectroscopic study of selected natural jarosites. *Spectrochim. Acta* **2006**, *63*, 1–8. [\[CrossRef\]](#)
29. Casas, J.M.; Paipa, C.; Godoy, I.; Vargas, T. Solubility of sodium-jarosite and solution speciation in the system $\text{Fe(III)}\text{--Na--H}_2\text{SO}_4\text{--H}_2\text{O}$ at 70 °C. *J. Geochem. Explor.* **2007**, *92*, 111–119. [\[CrossRef\]](#)
30. Murphy, P.J.; Smith, A.M.L.; Hudson-Edwards, K.A.; Dubbin, W.E.; Wright, K. Raman and IR spectroscopic studies of alunite-supergroup compounds containing Al, Cr^{3+} , Fe^{3+} and V^{3+} at the B site. *Can. Mineral.* **2009**, *47*, 663–681. [\[CrossRef\]](#)
31. Powers, D.A.; Rossman, G.R.; Schugar, H.F.; Gray, N.B. Magnetic behavior and infrared spectra of jarosite, basic iron sulfate, and their chromate analogs. *J. Solid State Chem.* **1975**, *13*, 1–13. [\[CrossRef\]](#)

Disclaimer/Publisher’s Note: The statements, opinions and data contained in all publications are solely those of the individual author(s) and contributor(s) and not of MDPI and/or the editor(s). MDPI and/or the editor(s) disclaim responsibility for any injury to people or property resulting from any ideas, methods, instructions or products referred to in the content.